Poverty Estimation Using a ConvLSTM-Based Model With Multisource Remote Sensing Data: A Case Study in Nigeria

Jie Tang, Xizhi Zhao, Fuhao Zhang, Agen Qiu, and Kunwang Tao

***Abstract*—Poverty is a global challenge, the effects of which are felt on the individual to national scale. To develop effective support policies to reduce poverty, local governments require precise poverty distribution data, which are lacking in many areas. In this study, we proposed a model to estimate poverty on a spatial scale of 10 × 10 km by combining features extracted from multiple data sources, including nighttime light remote sensing data, normalized difference vegetation index, surface reflectance, land cover type, and slope data, and applied the model to Nigeria. Considering that the trends of environmental factors contain valid information related to poverty, time-series features were extracted through convolutional long short-term memory and used for the assessment. The poverty level is represented by the wealth index derived from the Demographic and Health Survey Program. The model exhibited good ability to estimate poverty, with an R^2 of 0.73 between the actual and estimated wealth index in Nigeria in 2018. Applying the proposed model to poverty estimation for Nigeria in 2021 yielded an R^2 value of 0.69, indicating good generalization ability. To further validate model reliability, we compared the assessment results with high-resolution satellite imagery and a state-level multidimensional poverty index. We also investigated the impact of incorporating time-series features on the accuracy of poverty assessment. Results showed that the addition of time-series features increased the accuracy of poverty estimation from 0.64 to 0.73. The proposed method has valuable applications for estimating poverty at the grid scale in countries without such data.**

***Index Terms*—Convolutional long short-term memory (convLSTM), Nigeria, nighttime light (NTL), poverty, time-series features.**

I. Introduction

POVERTY is a global problem. According to the World Bank's 2022 World Development Report, the COVID-19 pandemic caused the global economy to experience its worst crisis in a century, and the global poverty rate rose for the first time in this generation [1]. Prior to the outbreak of COVID-19, 1.2 billion people in 111 developing nations were experiencing multidimensional poverty, according to the 2022 Global Multidimensional Poverty Index (MPI) report of the United Nations Development Program [2]. Thus, reducing poverty has long been a global priority, especially in developing countries [3]. Poverty has many adverse effects, including malnutrition, high infant mortality rates, poor life expectancy, food insecurity, and slow economic growth, which are particularly significant in sub-Saharan Africa [4]. Nigeria is the most populous country in Africa, with over 200 million inhabitants [5]. Despite its status as the world's fifth largest exporter of liquefied natural gas and its abundant oil and gas resources [6], Nigeria currently has 97 million people living in poverty, the second highest amount in the world after India [2]. Poverty has, therefore, become a major barrier to Nigeria's sustainable development. Although poverty has long been an issue in Nigeria, it has only worsened at an alarming rate in recent years [7]. The United Nations has set a target for ending extreme poverty through sustainable development by 2030 [8]; however, this goal is highly unrealistic for Nigeria unless effective measures are implemented immediately. Therefore, accurate poverty data are critical for enabling the Nigerian government to establish scientifically sound poverty reduction programs that are adapted to local conditions.

Poverty is defined as the inability of individuals or families to acquire fundamental necessities [9]. Indices, such as the gross domestic product (GDP), per-capita income, housing, education, and energy, have been frequently used to assess the poverty status of households or areas [10], [11]. Although a series of studies have provided detailed estimates of education, healthcare, and fixed assets in developing countries [12], [13], [14], [15], gaps still exist in the measurement of economic metrics, such as poverty. Traditional ways of poverty measurements largely rely on economic survey data. However, frequent economic surveys require substantial investment, estimated at $1 billion per year in low-income nations [16]. Furthermore, economic surveys are limited by their inability to cover the entire population and delayed data updates [17]. Therefore, the main barrier to identifying poverty is a lack of sufficient and trustworthy data [18].

Unlike typical statistical or survey data, remote sensing data are objective and stable sources of information that can be updated quickly [19]. Nighttime light (NTL) remote sensing data capture Earth's NTL from space and has been widely used to

Manuscript received 4 July 2023; revised 17 September 2023 and 1 December 2023; accepted 9 January 2024. Date of publication 15 January 2024; date of current version 24 January 2024. This work was supported in part by the National Natural Science Foundation of China under Grant 42201434, and in part by the Chinese Academy of Surveying and Mapping Basic Research Fund Program under Grant AR2204. *(Corresponding author: Xizhi Zhao.)*

The authors are with the Geospatial Big Data Application Research Center, Chinese Academy of Surveying and Mapping, Beijing 100830, China (e-mail: tangjiecasm@163.com; zxz@casm.ac.cn; zhangfh@casm.ac.cn; qiuag@casm.ac.cn; taokw@casm.ac.cn).

Digital Object Identifier 10.1109/JSTARS.2024.3353754

monitor human economic activities, such as impervious surfaces [20], food security [21], carbon dioxide emissions [22], urban development [23], [24], [25], [26], GDP [27], [28], electricity consumption [29], and population changes [30]. Because NTL intensity can effectively reflect the regional economic situation [31], it is commonly used for poverty assessments [32], [33], [34], [35]. For example, Lin et al. [36] used NTL data to observe and model dynamic changes in economic development in the Nile River Basin and verify that NTL data are a feasible alternative to large-scale economic surveys. Moreover, Yong et al. [37] integrated NTL data from the Defense Meteorological Satellite Program Operational Linescan System and National Polar-Orbiting Partnership Visible Infrared Imaging Radiometer Suite (VIIRS) to evaluate poverty status in southwestern China. However, these studies relied solely on NTL data as an information source and may have omitted other important poverty-related factors [38]. Furthermore, the brightness value of NTL is typically low in locations where living standards are near the poverty line, resulting in a negligible brightness difference. Therefore, NTL data alone cannot easily distinguish between economic activity levels in such locations [17].

To compensate for this shortcoming, some studies have attempted to incorporate additional data sources alongside NTL data. For example, Wang et al. [39] combined NTL data with land cover and digital elevation model (DEM) data to identify poverty levels in county-level administrative regions in China. Moreover, Shi et al. [40] developed a comprehensive poverty index by integrating NTL data, DEM, normalized difference vegetation index (NDVI), and point-of-interest (POI) data to generate a poverty map of Chongqing, China. Studies utilizing multiple data sources have achieved more accurate poverty assessments than those using only NTL data [40]. In current poverty assessment, NTL data [41] are often combined with other data, such as land cover data [39], [42], NDVI [43], [44], Google Earth imagery [17], [45], and DEM [40], [42], to enhance the accuracy of the assessment.

However, the features currently used for poverty estimation are limited to single temporal or attribute features and do not include time-series features. Time-series features can provide information regarding the long-term trends and development directions of an observed object [46], [47]. In many studies [48], [49], [50], [51], integrating different types of features proved crucial for improving model performance. The degree of poverty in a particular area is not only influenced by current environmental factors but also by past factors and their trends over time. For example, NTL brightness levels can reflect the construction of infrastructure, such as roads; however, although an increase in infrastructure construction may not immediately alleviate poverty, it may impact future poverty alleviation. Thus, an upward trend in the level of NTL brightness may indicate increasing construction of infrastructure and a greater likelihood of poverty alleviation. Therefore, the inclusion of time-series characteristics in poverty assessments can increase the variety of features, deliver the combined benefits of spatial and temporal data, and produce more accurate results.

Traditional methods for extracting time-series features include autoregressive integrated moving average models [52], [53], filter-based methods [54], [55], and support vector machines [56], all of which exhibit limitations when dealing with massive high-dimensional amounts of data [57]. However, creating an efficient machine-learning model necessitates extensive domain knowledge [58]. Deep learning models are capable of extracting higher dimension and more abstract latent features from data than traditional methods [58], performing autonomous learning from the data [59], and directly adapting to data without any prior assumptions [60]. Indeed, deep learning has been successfully applied to remote sensing because of its adaptability in feature representation and automation [61]. Deep learning models can accurately approximate complex nonlinear relationships and help extract time-series features from remote sensing images [59], [62]. Deep learning models have been used widely for extracting time-series features. For example, Chen et al. [48] used an attention mechanism in conjunction with long short-term memory (LSTM) to extract time-series features and predict the remaining service life of machinery. Chemali et al. [63] used a recurrent neural network (RNN) with LSTM to estimate the state of charge of lithium-ion batteries. Kisvari et al. [64] proposed a method for forecasting wind power generation that relies on a gated recursive deep learning model that extracts temporal features. Convolutional long short-term memory (ConvLSTM) is a spatial extension of LSTM that aims to extract spatiotemporal features from data by combining convolution operations [65]. Compared with RNN models, ConvLSTM not only alleviates gradient explosion and vanishing problems but also further extracts high-dimensional spatiotemporal features [65], [66].

This study proposes a ConvLSTM-based model to estimate poverty by combining features extracted from multiple data sources, including NTL remote sensing data, NDVI, surface reflectance, land cover type, and slope data. The primary contributions of this study are as follows.

1) This study introduces time-series features into a poverty assessment model. Poverty often exhibits continuity over time, with poverty in previous years affecting poverty in the present. In this study, we selected time-series features for inclusion in poverty-level analysis and integrated them with spatial features to enhance their diversity. By exploiting the advantages of these features, we ultimately improve the accuracy of poverty assessment.
2) We developed a ConvLSTM-based model to extract spatiotemporal features for poverty assessment. Compared with the traditional LSTM networks, ConvLSTM can extract temporal features while preserving the spatial features of remote sensing images. Therefore, we extracted the spatiotemporal features of NTL, NDVI, and surface reflectance using ConvLSTM and combined them with the spatial features of land cover and slope data obtained through convolution, creating a ConvLSTM feature fusion model. We then compared the evaluation results with and without the addition of temporal features, and confirmed that the inclusion of temporal features improves the accuracy of the poverty assessment model.
3) We generated a high-precision poverty map of Nigeria with a resolution of 10×10 km using the proposed poverty assessment model. This poverty map can reveal the spatial

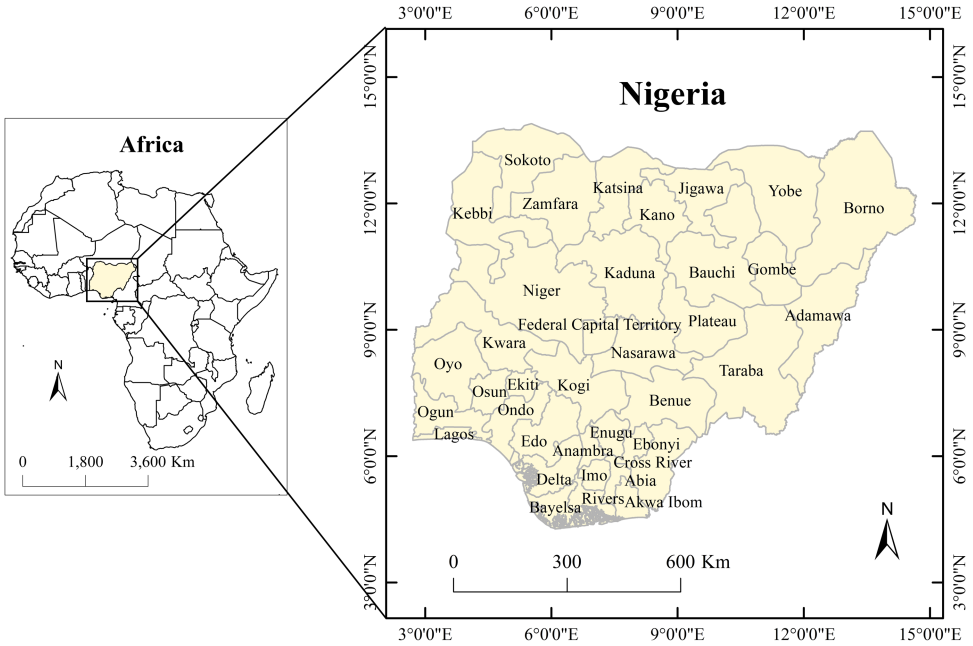

Fig. 1. Map of Nigeria.

distribution of poverty and assist local governments in formulating effective poverty reduction policies.

The rest of this article is organized as follows. Section II describes the study area, data sources, ConvLSTM network model structure, and the specific poverty assessment method. Section III presents the methods. Section IV presents the results and evaluates the model accuracy. Section V discusses the strengths and limitations of the study and further analyzes the impact of time-series features. Finally, Section VI concludes this article.

II. Study Area and Data

A. Study Area

Nigeria is located at the tip of Africa's west coast on the Gulf of Guinea and has abundant mineral resources, including coal, iron ore, and barite [67]. Nigeria is divided into 36 states and 1 Federal Capital Territory, covering 923 768 km^2 (see Fig. 1). According to data from the World Bank, Nigeria had a GDP of 44.083 billion U.S. dollars and a population of 213.4 million people in 2021, making it the largest economy and most populous country in Africa [68]. Despite its abundant natural and human resources, Nigeria continues to suffer from severe poverty, with significant disparity in economic development between the southern and northern regions. The southern region relies primarily on industries, such as manufacturing and petroleum, making it relatively wealthy, whereas the northern region, which relies mainly on agriculture and livestock, is relatively poor [69]. As a result, Nigeria's social and economic development exhibits clear spatial inequality. Overall, the Nigerian economy is characterized by an overdependence on the petroleum industry, with a single economic structure and major problems of poverty and wealth polarization [70].

B. Data

Seven different types of data were used in this study (see Fig. 2): demographic and health survey (DHS) wealth index (WI) data, NTL, surface reflectance, NDVI, slope, land cover, and administrative boundary data. WI was the dependent variable in the poverty estimation model, and the independent variables were derived from NTL, surface reflectance, NDVI, land cover type, and slope data. A background map was created using administrative boundary data.

The WI is a composite measure of a household's standard of living derived from the DHS survey [71], [72], which has previously been used to assess household poverty levels [73], [74], [75]. The WI is divided into integers ranging from 1 to 5, where 1 represents the poorest and 5 represents the richest. DHS surveys provide the geographical coordinates of household clusters, which are randomly offset by up to 5 km (1% of rural clusters have a maximum offset of 10 km) to safeguard the respondents' anonymity. To estimate poverty in Nigeria, the average result of the intracluster household WI was used as the WI of the cluster. We employed 2018 Nigerian survey data as the sample, which included 1382 household clusters of between 10 and 30 households, with a mean of 29.1 and a median of 30.

The annual VIIRS nighttime lights (VNL) V2 data from 2012 to 2018 released by the Earth Observation Group under the National Oceanic and Atmospheric Administration in the United States [76] were used to reflect the NTL intensity. The image element radiation values are given in nW/cm^2/sr, and the data have a resolution of 15 arc-sec (equator at 500 m).

NDVI, surface reflectance, and DEM data were derived from Google Earth Engine [77]. NDVI data were provided by the MOD13A1 V6.1 (MODIS/061/MOD13A1) with a data

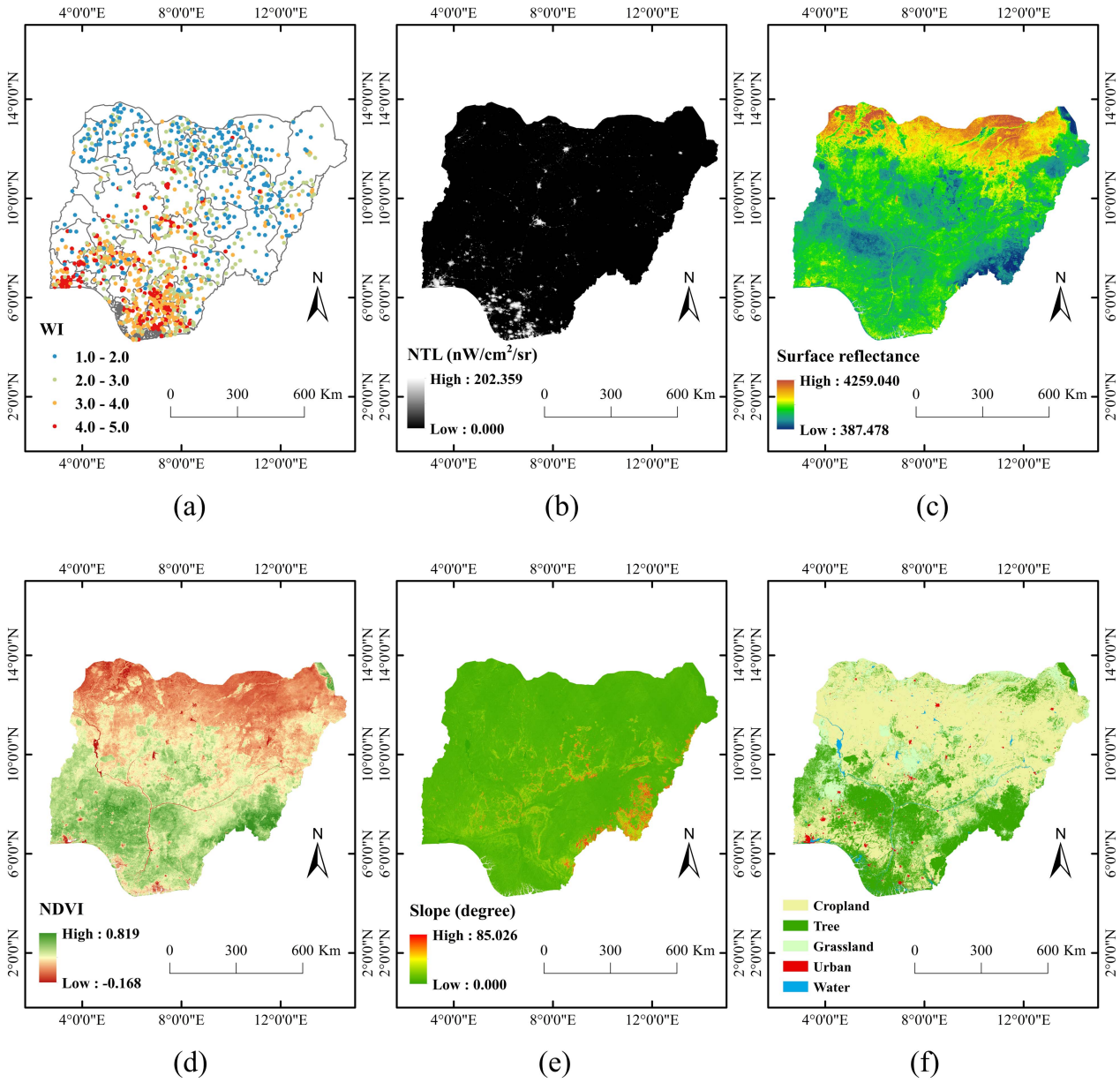

Fig. 2. Datasets used in this research. (a) WI map. (b) National polar-orbiting partnership VNL image. (c) Surface reflectance map. (d) NDVI map. (e) Slope map. (f) Land cover map.

resolution of 500 m. The MOD13A1 product is a 16-day composite dataset, and data from 2018 were averaged monthly to generate monthly data for this study. Surface reflectance data were obtained from MOD09A1 V6.1 (MODIS/061/MOD09A1). The MOD09A1 product comprises eight-day composite data with a data resolution of 500 m, corrected for atmospheric conditions, such as gases, aerosols, and Rayleigh scattering. To reflect changes in surface reflectance over the course of the year, monthly data for 2018 were generated using monthly averages of the sur_refl_b01 band (wavelength 620–670 nm) from the MOD09A1 product. Slope data were calculated using Google Earth Engine's Shuttle Radar Topography Mission V3 digital elevation product (USGS/SRTMGL1_003) with a resolution of 30 m.

Land cover data from 2018 at 300 m resolution, provided by the European Space Agency Climate Change Initiative project, were used to reflect the surface cover characteristics [78]. Administrative boundary vector data for Nigeria were obtained from the Database of Global Administrative Areas [79].

III. Methods

A. Feature Design

Poverty is a complex phenomenon that is influenced by several elements, including natural, social, and geographical factors. This study considered the selection of features from three perspectives: economic activities, surface morphology, and natural environment. Table I presents previous studies that

TABLE I
DATA USED IN POVERTY ASSESSMENT

Ref.	Year	Data
[40]	2020	NTL, DEM, NDVI, POI, survey data, and socioeconomic data.
[44]	2020	PlanetScope data, NDVI, and road map.
[42]	2021	NTL, DEM, land cover, Open Street Map road data, and socioeconomic statistics.
[43]	2022	NTL, Google Earth imagery, NDVI, and survey data (DHS and Living Standards Measurement Study).
[39]	2022	NTL, land cover, DEM, and socioeconomic statistics.
[83]	2022	Google Earth imagery (NTL, NDVI, land surface temperature, and rainfall data), Open Street Map (road map, POI, and built-up area), and census data.

used remote sensing data to estimate poverty. Among them, NTL data were most commonly used and are considered to accurately reflect the socioeconomic development status [80], [81], [82]. NDVI data exhibit strong seasonal variations that are closely related to crop yields and pasture conditions [43], which can indirectly reflect economic conditions. Surface reflectance provides a comprehensive reflection of surface conditions. Land cover data describe the land's usage types, whereas slope data capture information regarding terrain, landforms, and changes in elevation. Therefore, we ultimately determined five data types: NTL, surface reflectance, NDVI, slope, and land cover type, to construct the poverty assessment model.

As longer time intervals can better reflect economic development trends, NTL data were collected annually from 2012 to 2018 to form a time-series dataset. Considering the seasonal variation in vegetation and the surface environment, NDVI and surface reflectance data were collected monthly from January to December 2018. As the slope data and land cover data changed less frequently over time, these data were not used to construct the time series.

The above data have different spatial resolutions, with the NTL, NDVI, and surface reflectance data having a resolution of 500 m, the slope data having a resolution of 30 m, and the land cover data having a resolution of 300 m. To unify the resolution, slope and land cover data were resampled to a resolution of 500 m. Datasets consisting of each type of data were normalized to achieve a mean of zero and a standard deviation of one.

B. Extraction of Temporal Features by ConvLSTM

LSTM is an RNN modification that overcomes gradient explosion and disappearance problems caused by long-sequence training [84]. Unlike the traditional RNN model, LSTM has a special memory cell structure in which each memory cell consists of a cell state and a hidden state. The cell state is responsible for storing memory, whereas the hidden state is used to output information. The input, output, and forget gates of LSTM regulate the transmission and processing of information

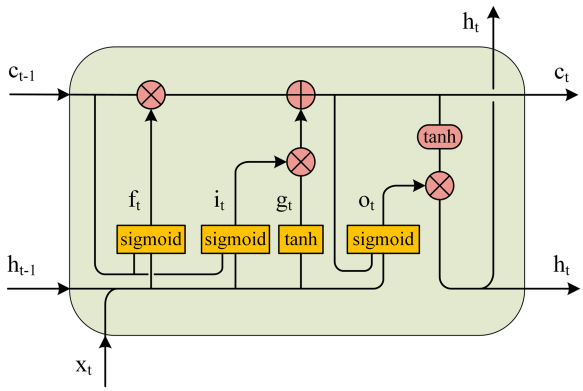

Fig. 3. Diagram of the ConvLSTM structure.

within a cell [85]. The input gate regulates the information stored in the cell, the output gate controls how the information is delivered to the next cell, and the forget gate determines the information that will be discarded. In LSTM, the information transfer mechanism of a cell unit is governed by the following equations:

$$i_t = \sigma\left(W_{xi}x_t + W_{hi}h_{t-1} + W_{ci} \circ c_{t-1} + b_i\right) \tag{1}$$

$$f_t = \sigma\left(W_{xf}x_t + W_{hf}h_{t-1} + W_{cf} \circ c_{t-1} + b_f\right) \tag{2}$$

$$c_t = f_t \circ c_{t-1} + i_t \circ \tanh\left(W_{xc}x_t + W_{hc}h_{t-1} + b_c\right) \tag{3}$$

$$o_t = \sigma\left(W_{xo}x_t + W_{ho}h_{t-1} + W_{co} \circ c_t + b_0\right) \tag{4}$$

$$h_t = o_t \circ \tanh\left(c_t\right) \tag{5}$$

where i_t represents the input gate, f_t represents the forget gate, and o_t represents the output gate. c_t represents the state at the current moment, c_{t-1} represents the state at the previous moment, h_t represents the final output, h_{t-1} represents the output at the previous moment, and x_t represents the input at the current moment. $W_{\cdot i}$ and b_i are the weights and biases of the input gates, $W_{\cdot f}$ and b_f are the weights and biases of the forgetting gates, and $W_{\cdot o}$ and b_o are the weights and biases of the output gates, respectively, where "$\cdot$" denotes x, h, and c, $\circ$ denotes the Hadamard product, and σ is the sigmoid function.

Although LSTM can successfully extract time-series features, it loses the spatial correlation and features of two-dimensional (2-D) data [65]. This is because the LSTM must flatten 2-D data into a 1-D vector when dealing with 2-D inputs. Shi et al. [65] suggested a modified LSTM called ConvLSTM to address this issue. The main distinction between ConvLSTM and LSTM is that ConvLSTM uses a convolution operation instead of matrix multiplication to facilitate the extraction of spatiotemporal features from the 2-D data (see Fig. 3) according to the following formulae:

$$i_t = \sigma\left(W_{xi} * X_t + W_{hi} * h_{t-1} + W_{ci} \circ c_{t-1} + b_i\right) \tag{6}$$

$$f_t = \sigma\left(W_{xf} * X_t + W_{hj} * h_{t-1} + W_{cf} \circ c_{t-1} + b_f\right) \tag{7}$$

$$c_t = f_t \circ c_{t-1} + i_t \circ \tanh\left(W_{xc} * X_t + W_{hc} * h_{t-1} + b_c\right) \tag{8}$$

$$o_t = \sigma\left(W_{xo} * X_t + W_{ho} * h_{t-1} + W_{co} \circ c_t + b_0\right) \tag{9}$$

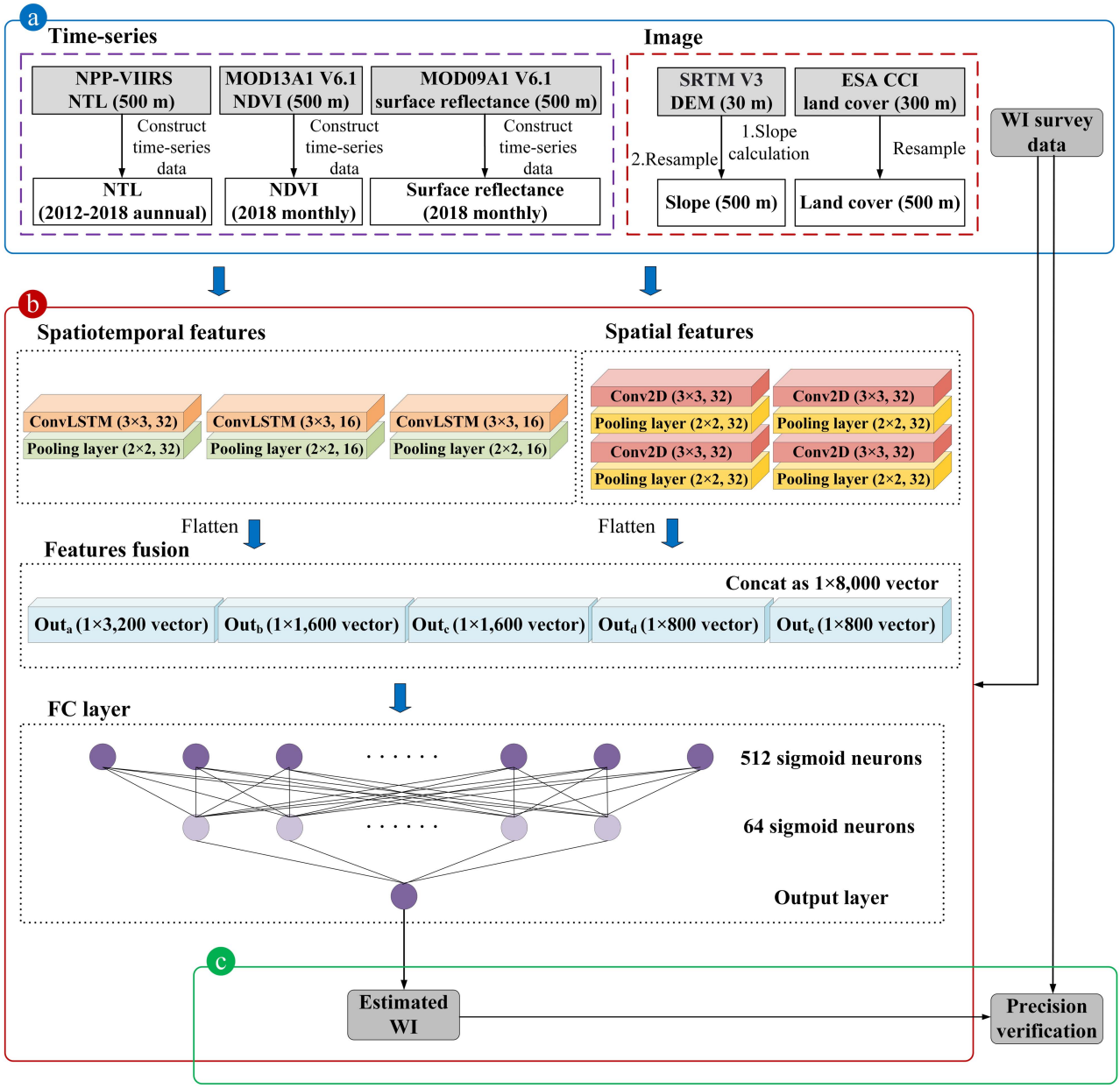

Fig. 4. Schematic of the poverty assessment model. (a) Data preprocessing. (b) Model structure. (c) Accuracy evaluation.

$$h_t = o_t \circ \tanh(c_t) \tag{10}$$

where $*$ denotes the convolution operator, W denotes a 2-D convolution filter with kernel $k \times k$, and k denotes the size of the convolution kernel. The remaining symbols are the same as those in LSTM. As convolutional computation and LSTM can extract spatial and time-series features, they are ideal for extracting spatiotemporal data for poverty estimation.

C. Structure of the Poverty Assessment Model

Because of the maximum 5-km offset for each household cluster location, a 10 × 10 km grid was generated with each cluster location as the center to ensure that the original location before the offset was within the study area. Subsequent poverty assessments were based on a 10 × 10 km grid as the basic research unit. The overall poverty assessment process is shown in Fig. 4, which includes the following aspects.

1) *Data preprocessing:* Slope data for the study area were derived from the DEM data. Slope and land cover data were resampled and processed to construct an image dataset, whereas NTL, NDVI, and surface reflectance data were used to build a time-series dataset.
2) *Model structure:* The poverty assessment estimation model proposed in this study was built based on ConvLSTM and convolutional layers. The multiple extracted features were integrated, and poverty assessment was performed through fully connected layers. Considering the strong correlation between NTL data and poverty levels, the number of channels for extracting the NTL data features using ConvLSTM was set to 32. The number of

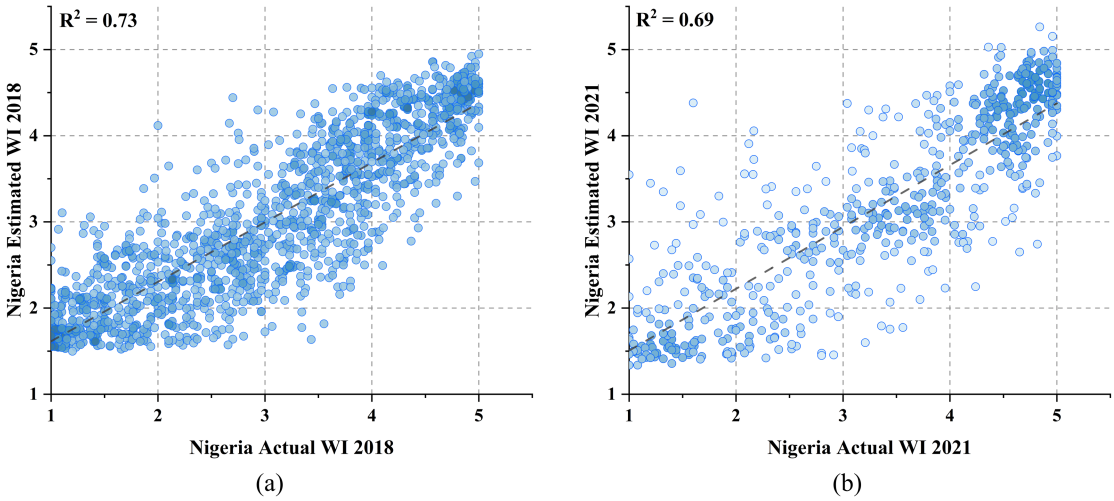

Fig. 5. Scatter plots of actual and estimated WI for Nigeria in (a) 2018 and (b) 2021.

channels for extracting the NDVI and surface reflectance data features using ConvLSTM was set to 16. The number of convolutional channels for extracting the slope and land cover data was set to 32. Detailed parameter settings and model architectures are shown in Fig. 4(b).

3) *Accuracy evaluation:* The model was trained using tenfold cross validation. The accuracy of the model was evaluated by calculating the R^2 value between the actual and estimated values. Subsequently, a trained model was used to estimate the poverty level of Nigerians in 2021 to prove its generalization performance. Furthermore, the accuracy of poverty estimation was validated by comparing the model results with high-resolution remote sensing imagery and a state-level MPI.

D. Training Methods

During the training process, the poverty assessment model was trained using the mean squared error (MSE) loss function and the stochastic gradient descent optimizer with momentum. The batch size was set to 16 and the model was trained for 200 epochs. MultiStepLR is a learning rate decay method used in PyTorch [86] that adjusts the learning rate at set intervals [87]. The initial learning rate was set to 0.01. Then, the MultiStepLR strategy was employed to adjust the learning rate, which was reduced by 50% every 20 epochs after 100 epochs of training. After multiple attempts, the aforementioned parameter settings achieved satisfactory results for the validation set. All models trained for 200 epochs were evaluated on the validation set, and the model with the highest R^2 was applied to the test set. To prevent overfitting and enhance the robustness and stability of the model, dropout layers were added to the fully connected layers, and image augmentation was performed using random flipping.

To test the performance of the poverty assessment model, tenfold cross validation was used to estimate the WI values for Nigeria in 2018. The 1382 household clusters in Nigeria were randomly divided into ten equally sized subsamples, with no overlap between the subsamples. We independently trained ten models, each with a different test set, with ten subsamples rotating as the test set. The remaining nine folds were used, with one fold as the validation set and eight folds as the training set. We trained the model on the training set and tuned its hyperparameters using a validation set. Finally, we evaluated the performance of the model on the test set using the coefficient of determination (R^2) between the actual and estimated values. The final poverty assessment model was applied to all regions of Nigeria to obtain WI estimates at a resolution of 10×10 km.

IV. Results

A. Accuracy Evaluation of the Poverty Estimation Model

The accuracy of the model was evaluated by calculating the R^2 value between the actual WI values and the estimated values for Nigeria, which was 0.73 [see Fig. 5(a)]. The R^2 value represents the proportion of the variance in the dependent variable that is predictable from the independent variable, with an R^2 of 0.73 indicating that the proposed poverty assessment model has good explanatory power for the level of poverty.

To further evaluate the generalizability of the model, we tested the applicability of the model developed using data from one year to the estimation of poverty in another. As the DHS provided WI data for Nigeria in 2021, we applied the model trained on data from 2018 to estimate the WI in 2021 and compared the results with the actual WI [see Fig. 5(b)]. An R^2 of 0.69 suggests a significant correlation between the actual and estimated values for Nigeria in 2021. Notably, the accuracy of the model was lower for 2021, which may be related to changes in the distribution pattern caused by Nigeria's economic development. However, the model exhibited a high overall level of accuracy, indicating its applicability across time dimensions and good generalization ability.

The poverty estimation results for Nigeria are shown in Fig. 6(b). The distribution structure of the poverty estimates was very similar to that of the true values [see Fig. 6(a)], indicating good performance of the proposed model. The range of the

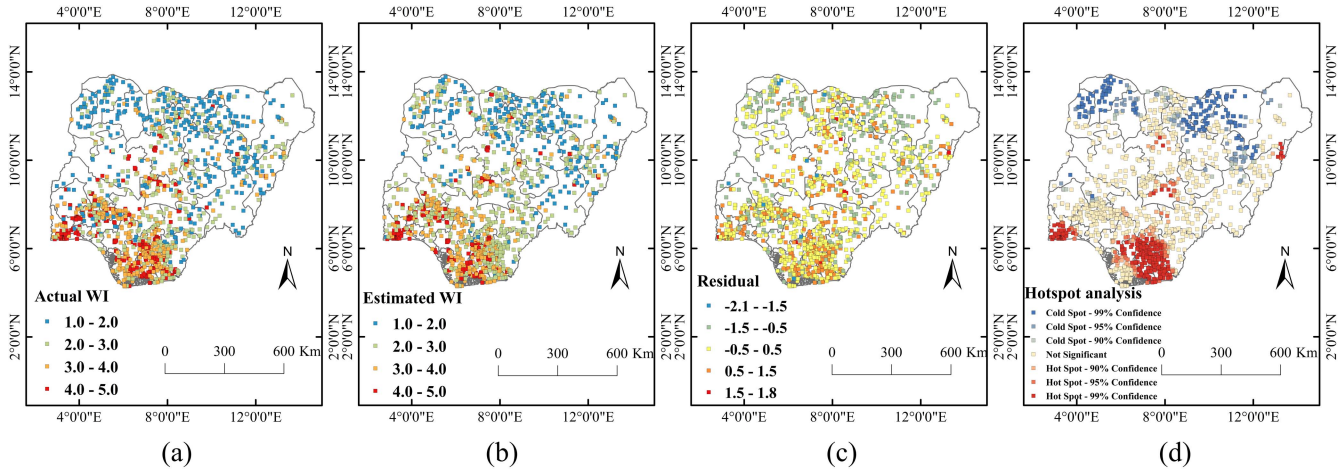

Fig. 6. Residual analysis results. (a) Actual WI. (b) Estimated WI. (c) Residual obtained from the true value minus the estimated value. (d) Residual hot spot analysis.

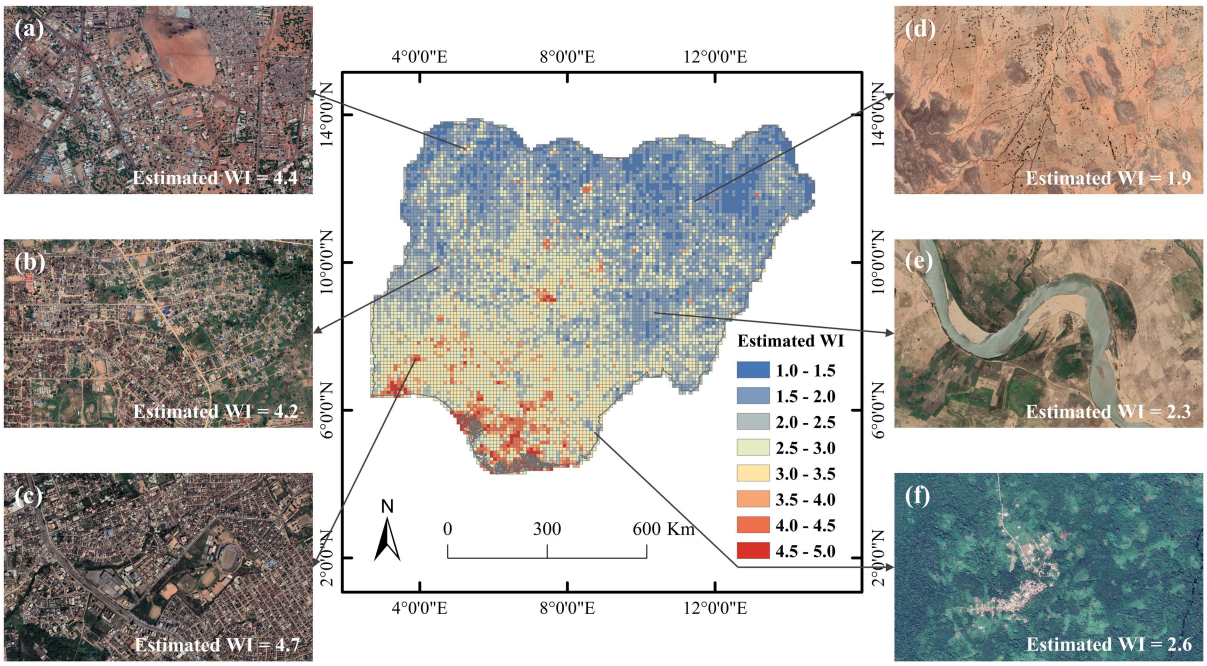

Fig. 7. Validation of poverty estimation results in Nigeria using Google Earth images.

actual WI was 1–5, whereas the range of the estimated WI was 1.50–4.95, which is smaller than the range of the true values. Fig. 6(c) displays the residuals obtained by subtracting the predicted values from the true values. Most of the residuals were between −0.5 and 0.5, indicating a small difference between the true and estimated values. Fig. 6(d) presents a hot spot analysis of the residuals between the actual and estimated values using the Getis-Ord (GI∗) method [88]. Hot spots were concentrated in high-value areas, and cold spots were concentrated in low-value areas. As the residuals were obtained by subtracting the estimated values from the actual values, the proposed model appeared to understate high values and overstate low values. This may be related to the use of the MSE as a loss function in the poverty estimation model. The MSE was less sensitive to deviations in the predicted results, and the model tended to bias the output toward the mean. The MSE loss function averages the impact of the outliers rather than increasing their influence.

B. Accuracy Verification by Comparison With High-Resolution Remote Sensing Images

A poverty map of Nigeria at a 10 × 10 km resolution was generated using the poverty estimation model, as shown in Fig. 7. Regions with higher WI values are displayed in red, whereas those with lower WI values are displayed in blue. Overall, the southern regions of Nigeria appeared more affluent, whereas the northern regions appeared less affluent. Previous research has indicated that visual comparisons using high-resolution remote

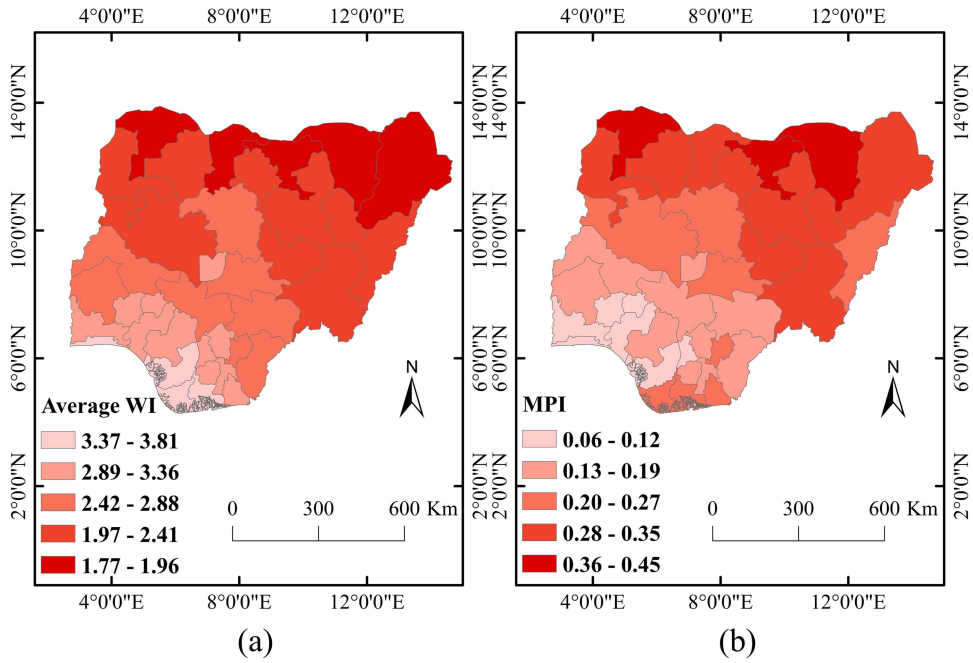

Fig. 8. Comparative analysis of average WI and MPI values. (a) State-level average WI. (b) State-level MPI.

sensing imagery can effectively validate assessment results. For example, Shi et al. [40] assessed the accuracy of poverty identification results through remote sensing imagery. Varshney et al. [89] evaluated the proportion of metal and thatched roofs using Google Earth imagery and considered villages with a higher proportion of thatched roofs as impoverished. Therefore, according to the previous research, we randomly selected three high-WI estimated points and three low-WI estimated points on the poverty map of Nigeria. We then visually validated the accuracy of the poverty assessment results using Google Earth. The estimated WI values for the points corresponding to Fig. 7(a)–(c) were 4.4, 4.2, and 4.7. According to Google Earth imagery, these three points are located in urban areas with complete road networks, which is consistent with the evaluation results of higher WI values. The estimated WI values for the points corresponding to Fig. 7(e) and (f) were 1.9, 2.3, and 2.6, respectively; these are located in wastelands and rural areas with no large buildings and inconvenient transportation, which is consistent with the evaluation results of lower WI values.

C. Accuracy Evaluation Through Comparison With the State-Level MPI

To further assess the accuracy of the model, we partitioned the generated poverty map of Nigeria based on different states and conducted regional statistical analysis. We calculated the mean of all poverty assessment values within each state as the average WI for that state. Then, the results were compared with the MPI provided by the 2018 Nigerian Human Development Report [90]. The MPI is an indicator developed by the United Nations Development Program in collaboration with the Oxford Poverty and Human Development Initiative to measure the severity of poverty [91]. The value of MPI ranges from 0 to 1, where a value closer to 0 denotes greater prosperity and a value closer to 1 denotes greater poverty. Fig. 8(a) shows the average WI for each state in Nigeria, with colors set using the natural breaks (Jenks) [92] method, where lighter colors represent affluence and darker colors represent poverty. Fig. 8(b) shows the MPI values for each state, again with the colors set using the natural breaks (Jenks) method. As shown in Fig. 8(a) and (b), the spatial distributions of the state-level average WI and MPI were very similar, both showing a pattern of affluence in the south and poverty in the north. Fig. 9 depicts the R^2 value between the average WI and MPI for each state in Nigeria, which was 0.66. This indicates that the estimated average WI can accurately explain the MPI and reflect the level of poverty in Nigeria.

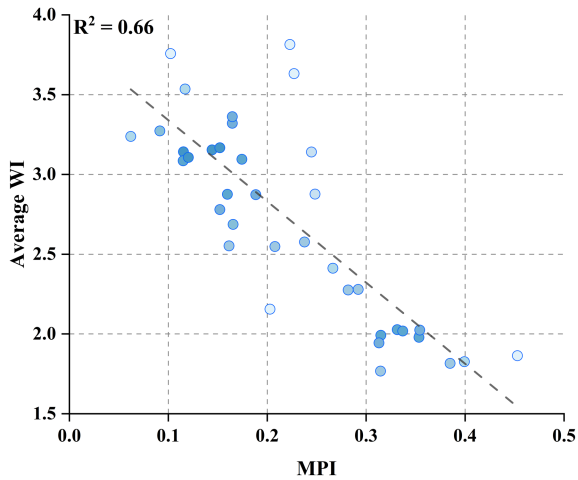

Fig. 9. Scatter plot of MPI and average WI values.

TABLE II
R^2 VALUES FOR FIVE DIFFERENT EVALUATION METHODS

	Method	R^2
1	Cubic polynomial model using only NTL data	0.36
2	CNN model using only NTL data	0.53
3	ConvLSTM model using only NTL time-series data	0.66
4	CNN features fusion model using five types of data	0.64
5	ConvLSTM feature fusion model using five types of data	0.73

TABLE III
R^2 VALUES FOR POVERTY ASSESSMENTS IN DIFFERENT LAND COVER TYPES

	Land cover type	Number of samples	R^2 without time-series features	R^2 with time-series features
1	Cropland	645	0.55	0.64
2	Tree	335	0.44	0.52
3	Grassland	90	0.61	0.69
4	Urban	301	0.39	0.41
5	Water	11	0.89	0.77

V. DISCUSSION

A. Effect of Including Time-Series Features on Model Accuracy

To investigate the effect of time-series features on poverty estimation, two sets of experiments were conducted with and without time-series features. The first used only NTL data, whereas the second used multiple data sources, including NTL, surface reflectance, NDVI, slope, and land cover. The model without time-series features extracted spatial features using only convolution. The R^2 values for each of the five models used for estimating the WI are shown in Table II. The cubic polynomial model using only NTL data to estimate WI had an R^2 of 0.36, the convolutional neural network (CNN) model using only NTL imagery as the model input had an R^2 of 0.53, and the ConvLSTM model using only NTL time-series data had an R^2 of 0.66. These results indicate that the inclusion of time-series features can effectively improve the accuracy of poverty assessment models when using a single data source. The ConvLSTM feature fusion model using five types of data achieved an R^2 of 0.73, which was significantly higher than the R^2 of 0.64 obtained by the CNN feature fusion model using five types of data. This indicates that, when using multiple data sources, incorporating time-series features can also improve the accuracy of the poverty assessment model. Therefore, we concluded that using multisource data and incorporating time-series features can effectively enhance the accuracy of poverty estimation in Nigeria.

B. Effect of Time-Series Features on Different Land Cover Types

The samples were classified based on the dominant land cover types within the sampling areas to analyze the impact of time-series features on the accuracy of poverty assessment for different land cover types. Both comparative models in Table III used the same five data sources: NTL, surface reflectance, NDVI, slope, and land cover type. The only difference was whether time-series features were included. The inclusion of time-series features significantly improved the accuracy of poverty assessment for the cropland, tree, and grassland land cover types. However, the addition of time-series data had a minimal impact on the accuracy of poverty assessment in urban areas. Moreover, incorporating time-series elements reduced the accuracy of evaluations in regions dominated by water. The improvement in accuracy for cropland, tree, and grassland areas may be attributed to their pronounced seasonal variation; time-series features can effectively capture such changes and provide rich information to support poverty assessments. In urban areas, where surface changes are minimal owing to the predominance of concrete structures, the addition of time-series features may not have a significant effect. In regions where water is the dominant land cover type, the ground structure is simple and exhibits little change over time; thus, incorporating time-series features may not provide significant additional information and rather introduce interference, leading to a reduction in assessment accuracy.

C. Poverty Reduction Recommendations

Based on the analysis results of this study, we proposed the following recommendations for local governments to reduce the poverty rate. First, we recommend increased infrastructure, such as roads, railways, bridges, and markets, in impoverished regions. The construction of roads can better connect impoverished areas within developed cities, providing more opportunities for poorer inhabitants. Well-maintained roads can also facilitate population mobility and commercial operations, making it easier for impoverished individuals to enter the job market and increase their income. Second, we suggest that local governments introduce water-saving agricultural technologies to promote the cultivation of drought-resistant crops. Some states in northern Nigeria are close to the Sahara Desert and face severe issues of drought and land desertification [93]. Agriculture is the primary economic activity in these areas, but drought restricts crop cultivation and livestock development, affecting agricultural output [94]. In addition, we suggest that local governments encourage economic diversification in rural areas, reducing dependence on agriculture and ultimately decreasing the poverty incidence rate.

D. Strengths and Limitations

In this study, we proposed a new poverty estimation model that combines spatial and temporal features extracted from multiple data sources, including NTL, surface reflectance, NDVI, slope, and land cover types. The use of multiple data sources enables a more comprehensive reflection of the local poverty situation than relying on a single data source. Moreover, the use of ConvLSTM

allows the extraction of temporal features while maintaining spatial characteristics, which enables the model to incorporate both temporal and spatial features. Furthermore, we generated a high-precision poverty map for Nigeria at a resolution of 10 $\times$ 10 km, which can serve as a valuable reference for local governments to formulate effective poverty alleviation policies.

Traditional economic survey data have long update cycles, are often expensive, and commonly lack detailed spatial information. Therefore, we proposed a poverty estimation method that utilizes existing publicly available data resources to achieve rapid and efficient poverty map updates. We further validated the positive impact of time-series features on the accuracy of poverty assessment. This expands the range of feature selections for poverty assessment.

In this study, we employed tenfold cross validation to evaluate the model and determined that the R^2 value between the actual and estimated WI values was 0.73. This indicates good performance of the proposed poverty estimation model. Similarly, Jean et al. [17] used a transfer learning method that utilizes features extracted from Google satellite imagery to assess the poverty status of Malawi, Rwanda, Uganda, and Nigeria at a spatial resolution of 10 km, and obtained R^2 values of 0.55, 0.75, 0.66, and 0.69, respectively. Yeh et al. [19] developed an end-to-end deep learning model using multispectral satellite imagery and NTL images as inputs for poverty assessment in 23 African countries. The model achieved an average R^2 of 0.7. Therefore, our proposed model is at a high level compared with previous studies.

To verify the effectiveness of the model, the model obtained by training with 2018 data was applied to 2021 survey data. After temporal migration, the accuracy of the model decreased slightly, with the R^2 dropping from 0.73 to 0.69. Overall, the model maintained good performance. The observed decline in accuracy could be related to changes in data distribution, as Nigeria's poverty patterns have changed over time. In addition, we analyzed the model's residuals and further validated its accuracy using Google satellite imagery and the MPI. Verification of the poverty assessment results from multiple perspectives demonstrated the reliability and accuracy of the model.

Although the poverty assessment model proposed in this study demonstrated accuracy and effectiveness in poverty estimation in Nigeria, some limitations should be addressed. First, because of the maximum offset of 5 km for the sampling clusters, we used a minimum research unit of 10 $\times$ 10 km to ensure that the true positions of the sampling points fell within the study area. However, because the positions of the sampling clusters were not accurate, the corresponding positions of the actual WI values were also inaccurate, which is an unavoidable error in this method. In addition, because of data source limitations, the resolution of the generated poverty estimation map is 10 $\times$ 10 km, which provides a relatively coarse poverty assessment. Second, the causes of poverty are very complex and are related not only to natural environmental factors but also to the government's organizational capabilities and the population characteristics. In this study, we only utilized a few types of data to construct the poverty estimation model, which may not fully capture all factors contributing to poverty development. In future research, more diverse data should be considered, such as POI, road network, and poverty survey data from other sources, to ensure a more comprehensive measurement. Third, because the DHS survey was conducted at the national level, the model was only trained on the 2018 DHS survey data for Nigeria and the poverty estimation map was only produced for Nigeria. Thus, future research should consider producing large-scale poverty estimation maps for multiple countries.

VI. Conclusion

Precise poverty distribution data, which are required to establish effective poverty reduction measures, are lacking in many parts of the world. Therefore, to achieve national wide poverty assessment and save labor and material resources, we proposed a ConvLSTM-based poverty estimation model using multiple remote sensing data obtained from publicly available datasets. We evaluated the proposed poverty estimation model for Nigeria and generated a poverty map with a resolution of 10 $\times$ 10 km. The model was evaluated using tenfold cross validation of 2018 DHS survey data, and the calculated R^2 value was 0.73, indicating good model performance.

Three methods were used to validate the effectiveness and accuracy of the model. First, the generalizability of the model was verified by applying the model trained on 2018 data to estimate the WI in 2021 and comparing the results with the actual WI. The R^2 value in 2021 was 0.69, indicating that our model maintained good performance after temporal transfer. Second, the poverty estimation results were visually evaluated at six randomly selected points using Google Earth imagery. Results showed that areas with higher WI values were in cities with convenient transportation, whereas areas with lower WI values were in remote and rural areas with inconvenient transportation. Furthermore, a comparison of the state-level averaged WI map with the state-level MPI map provided in the 2018 Nigeria Human Development Report was performed. The calculated R^2 between the MPI and state-level averaged WI was 0.66, indicating a strong correlation between the two maps.

To verify the improvement in poverty estimation accuracy achieved by adding time-series features, we trained four additional models for comparison. Among them, the CNN model using only NTL data had an R^2 value of 0.53, whereas the ConvLSTM model using only NTL time-series data had an R^2 value of 0.66. This demonstrates that adding time-series features can significantly improve the accuracy of the model when only NTL data are used. In addition the model using multiple data without time-series features had an R^2 value of 0.64, whereas the model using the same types of data with time-series features had an R^2 value of 0.73, further confirming that the addition of time-series features can significantly improve the accuracy of poverty estimation.

To analyze the impact of time-series features on poverty assessment across different land cover types, a comparative analysis was conducted by considering the inclusion or exclusion of time-series features. The results indicated that incorporating time-series information can improve the model accuracy in

cropland, tree, and grassland areas, but has a minimal impact on urban areas and may even lead to a decrease in assessment accuracy in regions dominated by water bodies.

In conclusion, we present a high-precision poverty assessment model that integrates time-series features and effectively utilizes publicly available remote sensing data for rapid and accurate spatial poverty assessment. The poverty maps generated by this method can help local governments gain detailed insights into poverty distribution and formulate targeted policies to alleviate poverty.

REFERENCES

[1] World Bank, *World Development Report 2022: Finance for an Equitable Recovery*. Washington, DC, USA: World Bank, 2022.

[2] "2022 global multidimensional poverty index (MPI)," United Nations Development Programme, New York, NY, USA, 2022.

[3] X. Zhao et al., "Estimation of poverty using random forest regression with multi-source data: A case study in Bangladesh," *Remote Sens.*, vol. 11, no. 4, Feb. 2019, Art. no. 375, doi: 10.3390/rs11040375.

[4] E. Murray, "Dumfries & galloway poverty and inequalities strategy," Accessed on: Dec. 16, 2022. [Online]. Available: https://www.dumgal.gov.uk/media/25837/Poverty-and-Inequalities-Strategy/pdf/Dumfries-and-Galloway-Poverty-and-Inequalities-Strategy-2021-2026_-FINAL.pdf?m=637848410572900000

[5] "World population prospects 2022: Summary of results," United Nations, New York, NY, USA, 2022.

[6] EIA, "Nigeria energy data," Accessed on: Mar. 15, 2023. [Online]. Available: https://www.eia.gov/international/overview/country/NGA

[7] R. Adeleke, O. Alabede, M. Joel, and E. Ashibuogwu, "Exploring the geographical variations and influencing factors of poverty in Nigeria," *Regional Sci. Policy Pract.*, vol. 15, no. 6, pp. 1182–1197, 2023, doi: 10.1111/rsp3.12621.

[8] "Transforming our world: The 2030 agenda for sustainable development," United Nations, New York, NY, USA, 2015.

[9] J. Haushofer and E. Fehr, "On the psychology of poverty," *Science*, vol. 344, no. 6186, pp. 862–867, May 2014, doi: 10.1126/science.1232491.

[10] I. U. Padda and A. Hameed, "Estimating multidimensional poverty levels in rural Pakistan: A contribution to sustainable development policies," *J. Cleaner Prod.*, vol. 197, pp. 435–442, Oct. 2018, doi: 10.1016/j.jclepro.2018.05.224.

[11] J. P. Gouveia, J. Seixas, and G. Long, "Mining households' energy data to disclose fuel poverty: Lessons for Southern Europe," *J. Cleaner Prod.*, vol. 178, pp. 534–550, Mar. 2018, doi: 10.1016/j.jclepro.2018.01.021.

[12] L. S. Tusting et al., "Mapping changes in housing in sub-Saharan Africa from 2000 to 2015," *Nature*, vol. 568, no. 7752, pp. 391–394, Apr. 2019, doi: 10.1038/s41586-019-1050-5.

[13] A. Osgood-Zimmerman et al., "Mapping child growth failure in Africa between 2000 and 2015," *Nature*, vol. 555, no. 7694, pp. 41–47, Mar. 2018, doi: 10.1038/nature25760.

[14] R. C. Reiner et al., "Variation in childhood diarrheal morbidity and mortality in Africa, 2000-2015," *New England J. Med.*, vol. 379, no. 12, pp. 1128–1138, Sep. 2018, doi: 10.1056/NEJMoa1716766.

[15] N. Graetz et al., "Mapping local variation in educational attainment across Africa," *Nature*, vol. 555, no. 7694, pp. 48–53, Mar. 2018, doi: 10.1038/nature25761.

[16] Sustain. Develop. Solutions Network, "Data for development: A needs assessment for SDG monitoring and statistical capacity development," New York, NY, USA, 2015.

[17] N. Jean, M. Burke, M. Xie, W. M. Davis, D. B. Lobell, and S. Ermon, "Combining satellite imagery and machine learning to predict poverty," *Science*, vol. 353, no. 6301, pp. 790–794, Aug. 2016, doi: 10.1126/science.aaf7894.

[18] Q. Ren, Q. X. Huang, C. Y. He, M. Z. Tu, and X. Y. Liang, "The poverty dynamics in rural China during 2000-2014: A multi-scale analysis based on the poverty gap index," *J. Geographical Sci.*, vol. 28, no. 10, pp. 1427–1443, Oct. 2018, doi: 10.1007/s11442-018-1554-1.

[19] C. Yeh et al., "Using publicly available satellite imagery and deep learning to understand economic well-being in Africa," *Nature Commun.*, vol. 11, no. 1, May 2020, Art. no. 2583, doi: 10.1038/s41467-020-16185-w.

[20] Y. Li et al., "Evaluating the ability of NOAA-20 monthly composite data for socioeconomic indicators estimation and urban area extraction," *IEEE J. Sel. Topics Appl. Earth Observ. Remote Sens.*, vol. 15, pp. 1837–1845, Feb. 2022, doi: 10.1109/jstars.2022.3149028.

[21] X. Y. Li et al., "Civil war hinders crop production and threatens food security in Syria," *Nature Food*, vol. 3, no. 1, pp. 38–46, Jan. 2022, doi: 10.1038/s43016-021-00432-4.

[22] X. P. Liu et al., "Estimating spatiotemporal variations of city-level energy-related CO_2 emissions: An improved disaggregating model based on vegetation adjusted nighttime light data," *J. Cleaner Prod.*, vol. 177, pp. 101–114, Mar. 2018, doi: 10.1016/j.jclepro.2017.12.197.

[23] Z. Chen, B. Yu, Y. Hu, C. Huang, K. Shi, and J. Wu, "Estimating house vacancy rate in metropolitan areas using NPP-VIIRS nighttime light composite data," *IEEE J. Sel. Topics Appl. Earth Observ. Remote Sens.*, vol. 8, no. 5, pp. 2188–2197, May 2015, doi: 10.1109/jstars.2015.2418201.

[24] C. Wang et al., "Evolution of urban spatial clusters in China: A graph-based method using nighttime light data," *Ann. Amer. Assoc. Geographers*, vol. 112, no. 1, pp. 56–77, Jan. 2022, doi: 10.1080/24694452.2021.1914538.

[25] Y. Tu, Z. Chen, C. Wang, B. Yu, and B. Liu, "Quantitative analysis of urban polycentric interaction using nighttime light data: A case study of Shanghai, China," *IEEE J. Sel. Topics Appl. Earth Observ. Remote Sens.*, vol. 15, pp. 1114–1122, Jan. 2022, doi: 10.1109/jstars.2021.3137167.

[26] Z. Chen et al., "Mapping global urban areas from 2000 to 2012 using time-series nighttime light data and MODIS products," *IEEE J. Sel. Topics Appl. Earth Observ. Remote Sens.*, vol. 12, no. 4, pp. 1143–1153, Apr. 2019, doi: 10.1109/jstars.2019.2900457.

[27] J. Sun, L. Di, Z. Sun, J. Wang, and Y. Wu, "Estimation of GDP using deep learning with NPP-VIIRS imagery and land cover data at the county level in CONUS," *IEEE J. Sel. Topics Appl. Earth Observ. Remote Sens.*, vol. 13, pp. 1400–1415, Mar. 2020, doi: 10.1109/jstars.2020.2983331.

[28] K. Shi, Y. Wu, D. Li, and X. Li, "Population, GDP, and carbon emissions as revealed by SNPP-VIIRS nighttime light data in China with different scales," *IEEE Geosci. Remote Sens. Lett.*, vol. 19, Aug. 2022, Art. no. 3008005, doi: 10.1109/lgrs.2022.3195266.

[29] K. F. Shi et al., "Evaluating spatiotemporal patterns of urban electricity consumption within different spatial boundaries: A case study of Chongqing, China," *Energy*, vol. 167, pp. 641–653, Jan. 2019, doi: 10.1016/j.energy.2018.11.022.

[30] S. Yu, Z. Zhang, and F. Liu, "Monitoring population evolution in China using time-series DMSP/OLS nightlight imagery," *Remote Sens.*, vol. 10, no. 2, Feb. 2018, Art. no. 194, doi: 10.3390/rs10020194.

[31] Z. Chen et al., "New nighttime light landscape metrics for analyzing urban-rural differentiation in economic development at township: A case study of Fujian province, China," *Appl. Geogr.*, vol. 150, 2023, Art. no. 102841.

[32] C. D. Elvidge et al., "A global poverty map derived from satellite data," *Comput. Geosci.*, vol. 35, no. 8, pp. 1652–1660, Aug. 2009, doi: 10.1016/j.cageo.2009.01.009.

[33] A. M. Noor, V. A. Alegana, P. W. Gething, A. J. Tatem, and R. W. Snow, "Using remotely sensed night-time light as a proxy for poverty in Africa," *Popul. Health Metrics*, vol. 6, no. 1, 2008, Art. no. 5.

[34] L. Zhang, X. Li, and F. Chen, "Spatiotemporal analysis of Venezuela's nighttime light during the socioeconomic crisis," *IEEE J. Sel. Topics Appl. Earth Observ. Remote Sens.*, vol. 13, pp. 2396–2408, May 2020, doi: 10.1109/jstars.2020.2995695.

[35] B. Yu, K. Shi, Y. Hu, C. Huang, Z. Chen, and J. Wu, "Poverty evaluation using NPP-VIIRS nighttime light composite data at the county level in China," *IEEE J. Sel. Topics Appl. Earth Observ. Remote Sens.*, vol. 8, no. 3, pp. 1217–1229, Mar. 2015, doi: 10.1109/jstars.2015.2399416.

[36] Y. Lin, T. H. Zhang, X. Q. Liu, J. Yu, J. A. T. Li, and K. Y. Gao, "Dynamic monitoring and modeling of the growth-poverty-inequality trilemma in the Nile River Basin with consistent night-time data (2000-2020)," *Int. J. Appl. Earth Observ. Geoinf.*, vol. 112, Aug. 2022, Art. no. 102903, doi: 10.1016/j.jag.2022.102903.

[37] Z. Yong et al., "Integrating DMSP-OLS and NPP-VIIRS nighttime light data to evaluate poverty in Southwestern China," *Remote Sens.*, vol. 14, no. 3, Feb. 2022, Art. no. 600, doi: 10.3390/rs14030600.

[38] G. E. Li, Z. L. Cai, X. J. Liu, J. Liu, and S. L. Su, "A comparison of machine learning approaches for identifying high-poverty counties: Robust features of DMSP/OLS night-time light imagery," *Int. J. Remote Sens.*, vol. 40, no. 15, pp. 5716–5736, Aug. 2019, doi: 10.1080/01431161.2019.1580820.

[39] M. Wang, Y. Wang, F. Teng, S. Li, Y. Lin, and H. Cai, "China's poverty assessment and analysis under the framework of the UN SDGs based on multisource remote sensing data," *Geo-Spatial Inf. Sci.*, pp. 1–21, 2022, doi: 10.1080/10095020.2022.2108346.

[40] K. F. Shi, Z. J. Chang, Z. Q. Chen, J. P. Wu, and B. L. Yu, "Identifying and evaluating poverty using multisource remote sensing and point of interest (POI) data: A case study of Chongqing, China," *J. Cleaner Prod.*, vol. 255, May 2020, Art. no. 120245, doi: 10.1016/j.jclepro.2020.120245.

[41] N. Z. Zhao, G. F. Cao, W. Zhang, E. L. Samson, and Y. Chen, "Remote sensing and social sensing for socioeconomic systems: A comparison study between nighttime lights and location-based social media at the 500 m spatial resolution," *Int. J. Appl. Earth Observ. Geoinf.*, vol. 87, May 2020, Art. no. 102058, doi: 10.1016/j.jag.2020.102058.

[42] Y. J. Wang, M. J. Wang, B. Huang, S. C. Li, and Y. H. Lin, "Evaluation and analysis of poverty-stricken counties under the framework of the UN sustainable development goals: A case study of Hunan Province, China," *Remote Sens.*, vol. 13, no. 23, Dec. 2021, Art. no. 4778, doi: 10.3390/rs13234778.

[43] B. Tang, Y. Y. Liu, and D. S. Matteson, "Predicting poverty with vegetation index," *Appl. Econ. Perspectives Policy*, vol. 44, no. 2, pp. 930–945, Jun. 2022, doi: 10.1002/aepp.13221.

[44] T. Stark, M. Wurm, X. X. Zhu, and H. Taubenbock, "Satellite-based mapping of urban poverty with transfer-learned slum morphologies," *IEEE J. Sel. Topics Appl. Earth Observ. Remote Sens.*, vol. 13, pp. 5251–5263, Aug. 2020, doi: 10.1109/jstars.2020.3018862.

[45] Y. X. Jiang et al., "Evaluation of county-level poverty alleviation progress by deep learning and satellite observations," *Big Earth Data*, vol. 5, no. 4, pp. 576–592, Nov. 2021, doi: 10.1080/20964471.2021.1967259.

[46] Z. Zhu and C. E. Woodcock, "Continuous change detection and classification of land cover using all available Landsat data," *Remote Sens. Environ.*, vol. 144, pp. 152–171, Mar. 2014, doi: 10.1016/j.rse.2014.01.011.

[47] J. X. Zhang and S. Y. Li, "Air quality index forecast in Beijing based on CNN-LSTM multi-model," *Chemosphere*, vol. 308, Dec. 2022, Art. no. 136180, doi: 10.1016/j.chemosphere.2022.136180.

[48] Z. Chen, M. Wu, R. Zhao, F. Guretno, R. Yan, and X. Li, "Machine remaining useful life prediction via an attention-based deep learning approach," *IEEE Trans. Ind. Electron.*, vol. 68, no. 3, pp. 2521–2531, Mar. 2021, doi: 10.1109/tie.2020.2972443.

[49] D. Hong, L. Gao, J. Yao, B. Zhang, A. Plaza, and J. Chanussot, "Graph convolutional networks for hyperspectral image classification," *IEEE Trans. Geosci. Remote Sens.*, vol. 59, no. 7, pp. 5966–5978, Jul. 2021, doi: 10.1109/tgrs.2020.3015157.

[50] L. Huang et al., "Multi-scale feature fusion convolutional neural network for indoor small target detection," *Front. Neurorobot.*, vol. 16, May 2022, Art. no. 881021, doi: 10.3389/fnbot.2022.881021.

[51] N. Zeng, P. Wu, Z. Wang, H. Li, W. Liu, and X. Liu, "A small-sized object detection oriented multi-scale feature fusion approach with application to defect detection," *IEEE Trans. Instrum. Meas.*, vol. 71, Feb. 2022, Art. no. 3507014, doi: 10.1109/tim.2022.3153997.

[52] C. Liu, S. C. H. Hoi, P. Zhao, and J. Sun, "Online ARIMA algorithms for time series prediction," in *Proc. 30th AAAI Conf. Artif. Intell.*, 2016, pp. 1867–1873.

[53] A. A. Adebiyi, A. O. Adewumi, and C. K. Ayo, "Comparison of ARIMA and artificial neural networks models for stock price prediction," *J. Appl. Math.*, vol. 2014, 2014, Art. no. 614342, doi: 10.1155/2014/614342.

[54] X. D. Wu and Y. N. Wang, "Extended and unscented Kalman filtering based feedforward neural networks for time series prediction," *Appl. Math. Model.*, vol. 36, no. 3, pp. 1123–1131, Mar. 2012, doi: 10.1016/j.apm.2011.07.052.

[55] T. W. Joo and S. B. Kim, "Time series forecasting based on wavelet filtering," *Expert Syst. Appl.*, vol. 42, no. 8, pp. 3868–3874, May 2015, doi: 10.1016/j.eswa.2015.01.026.

[56] Z. Y. Han, Y. Liu, J. Zhao, and W. Wang, "Real time prediction for converter gas tank levels based on multi-output least square support vector regressor," *Control Eng. Pract.*, vol. 20, no. 12, pp. 1400–1409, Dec. 2012, doi: 10.1016/j.conengprac.2012.08.006.

[57] Y. Bengio and Y. LeCun, "Scaling learning algorithms towards AI," in *Large-Scale Kernel Machines*. Cambridge, MA, USA: MIT Press, 2007.

[58] Z. Han, J. Zhao, H. Leung, K. F. Ma, and W. Wang, "A review of deep learning models for time series prediction," *IEEE Sensors J.*, vol. 21, no. 6, pp. 7833–7848, Mar. 2021, doi: 10.1109/jsen.2019.2923982.

[59] Y. LeCun, Y. Bengio, and G. Hinton, "Deep learning," *Nature*, vol. 521, no. 7553, pp. 436–444, 2015.

[60] P. Lara-Benitez, M. Carranza-Garcia, J. Garcia-Gutierrez, and J. C. Riquelme, "Asynchronous dual-pipeline deep learning framework for online data stream classification," *Integr. Comput.-Aided Eng.*, vol. 27, no. 2, pp. 101–119, 2020, doi: 10.3233/ica-200617.

[61] P. Dou, H. F. Shen, Z. W. Li, and X. B. Guan, "Time series remote sensing image classification framework using combination of deep learning and multiple classifiers system," *Int. J. Appl. Earth Observ. Geoinf.*, vol. 103, Dec. 2021, Art. no. 102477, doi: 10.1016/j.jag.2021.102477.

[62] Y. Bengio, A. Courville, and P. Vincent, "Representation learning: A review and new perspectives," *IEEE Trans. Pattern Anal. Mach. Intell.*, vol. 35, no. 8, pp. 1798–1828, Aug. 2013, doi: 10.1109/tpami.2013.50.

[63] E. Chemali, P. J. Kollmeyer, M. Preindl, R. Ahmed, and A. Emadi, "Long short-term memory networks for accurate state-of-charge estimation of Li-ion batteries," *IEEE Trans. Ind. Electron.*, vol. 65, no. 8, pp. 6730–6739, Aug. 2018, doi: 10.1109/tie.2017.2787586.

[64] A. Kisvari, Z. Lin, and X. L. Liu, "Wind power forecasting—A data-driven method along with gated recurrent neural network," *Renewable Energy*, vol. 163, pp. 1895–1909, Jan. 2021, doi: 10.1016/j.renene.2020.10.119.

[65] X. Shi, Z. Chen, H. Wang, D.-Y. Yeung, W.-K. Wong, and W.-C. Woo, "Convolutional LSTM network: A machine learning approach for precipitation nowcasting," in *Proc. 28th Int. Conf. Neural Inf. Process. Syst.*, 2015, pp. 802–810.

[66] L. Zhang, G. Zhu, P. Shen, J. Song, S. A. Shah, and M. Bennamoun, "Learning spatiotemporal features using 3DCNN and convolutional LSTM for gesture recognition," in *Proc. IEEE Int. Conf. Comput. Vis. Workshops*, 2017, pp. 3120–3128, doi: 10.1109/iccvw.2017.369.

[67] S. N. Asoegwu, *Leveraging Food Security Challenges in Nigeria: Through Agricultural Production, Processing and Storage for Mitigating Economic Recession*. Owerri, Nigeria: Federal University of Technology, Owerri Press, 2018, pp. 2–5.

[68] "Nigeria," World Bank, Accessed on: Feb. 19, 2023. [Online]. Available: https://data.worldbank.org/country/Nigeria

[69] A. O. Jaiyeola and I. Choga, "Assessment of poverty incidence in Northern Nigeria," *J. Poverty*, vol. 25, no. 2, pp. 155–172, Feb. 2021, doi: 10.1080/10875549.2020.1783424.

[70] A. E. Longe, O. O. Adelokun, and O. Omitogun, "The current account and oil price fluctuations nexus in Nigeria," *J. Competitiveness*, vol. 10, no. 2, pp. 118–131, Jun. 2018, doi: 10.7441/joc.2018.02.08.

[71] ICF, "The DHS program," Accessed on: Nov. 11, 2022. [Online]. Available: https://dhsprogram.com/data/

[72] S. O. Rutstein, "The DHS wealth index: Approaches for rural and urban areas," Macro Int. Inc., Irvine, CA, USA, 2008.

[73] M. A. Islam, N. J. Sathi, M. T. Hossain, A. Jabbar, A. M. N. Renzaho, and S. M. S. Islam, "Caesarean delivery and its association with educational attainment, wealth index, and place of residence in sub-Saharan Africa: A meta-analysis," *Sci. Rep.*, vol. 12, no. 1, Apr. 2022, Art. no. 5554, doi: 10.1038/s41598-022-09567-1.

[74] I. McCallum et al., "Estimating global economic well-being with unlit settlements," *Nature Commun.*, vol. 13, no. 1, May 2022, Art. no. 2459, doi: 10.1038/s41467-022-30099-9.

[75] S. Di Falco and G. Lynam, "New evidence on the rural poverty and energy choice relationship," *Sci. Rep.*, vol. 13, no. 1, 2023, Art. no. 3320.

[76] C. D. Elvidge, M. Zhizhin, T. Ghosh, F. C. Hsu, and J. Taneja, "Annual time series of global VIIRS nighttime lights derived from monthly averages: 2012 to 2019," *Remote Sens.*, vol. 13, no. 5, Mar. 2021, Art. no. 922, doi: 10.3390/rs13050922.

[77] "Google Earth Engine," Accessed on: Nov. 21, 2022. [Online]. Available: https://earthengine.google.com/

[78] "European space agency climate change initiative land cover," Accessed on: Nov. 25, 2022. [Online]. Available: http://maps.elie.ucl.ac.be/CCI/viewer/

[79] "Database of global administrative areas," Accessed on: Dec. 10, 2022. [Online]. Available: https://gadm.org/

[80] S. A. Frick, A. Rodriguez-Pose, and M. D. Wong, "Toward economically dynamic special economic zones in emerging countries," *Econ. Geogr.*, vol. 95, no. 1, pp. 30–64, Jan. 2019, doi: 10.1080/00130095.2018.1467732.

[81] J. V. Henderson, A. Storeygard, and D. N. Weil, "Measuring economic growth from outer space," *Amer. Econ. Rev.*, vol. 102, no. 2, pp. 994–1028, 2012.

[82] X. Chen and W. D. Nordhaus, "Using luminosity data as a proxy for economic statistics," *Proc. Nat. Acad. Sci.*, vol. 108, no. 21, pp. 8589–8594, 2011.

[83] N. Puttanapong, A. Martinez, J. A. N. Bulan, M. Addawe, R. L. Durante, and M. Martillan, "Predicting poverty using geospatial data in Thailand," *ISPRS Int. J. Geo-Inf.*, vol. 11, no. 5, May 2022, Art. no. 293, doi: 10.3390/ijgi11050293.

[84] Z. C. Lipton, J. Berkowitz, and C. Elkan, "A critical review of recurrent neural networks for sequence learning," Oct. 2015, *arXiv:1506.00019*.

[85] S. Hochreiter and J. Schmidhuber, "Long short-term memory," *Neural Comput.*, vol. 9, no. 8, pp. 1735–1780, Nov. 1997, doi: 10.1162/neco.1997.9.8.1735.
[86] R. X. Ma, J. Y. Lou, P. Li, and J. Gao, "Reconstruction of generative adversarial networks in cross modal image generation with canonical polyadic decomposition," *Wireless Commun. Mobile Comput.*, vol. 2021, Apr. 2021, Art. no. 8868781, doi: 10.1155/2021/8868781.
[87] X. Xie, Y. Liu, Y. Sun, G. G. Yen, B. Xue, and M. Zhang, "BenchENAS: A benchmarking platform for evolutionary neural architecture search," *IEEE Trans. Evol. Comput.*, vol. 26, no. 6, pp. 1473–1485, Dec. 2022, doi: 10.1109/tevc.2022.3147526.
[88] A. Getis and J. K. Ord, "The analysis of spatial association by use of distance statistics," in *Perspectives on Spatial Data Analysis*, L. Anselin and S. J. Rey, Eds. Berlin, Germany: Springer, 2010, pp. 127–145.
[89] K. R. Varshney et al., "Targeting villages for rural development using satellite image analysis," *Big Data*, vol. 3, no. 1, pp. 41–53, Mar. 2015, doi: 10.1089/big.2014.0061.
[90] "National human development report 2018: Nigeria," United Nations Development Programme, New York, NY, USA, 2018.
[91] "Global multidimensional poverty index," Accessed on: Jan. 22, 2023. [Online]. Available: https://ophi.org.uk/multidimensional-poverty-index
[92] C. A. Brewer and L. Pickle, "Evaluation of methods for classifying epidemiological data on choropleth maps in series," *Ann. Assoc. Amer. Geographers*, vol. 92, no. 4, pp. 662–681, Dec. 2002, doi: 10.1111/1467-8306.00310.
[93] N. I. Medugu, M. R. Majid, and F. Johar, "Drought and desertification management in arid and semi-arid zones of Northern Nigeria," *Manage. Environ. Qual.*, vol. 22, no. 5, pp. 595–611, 2011, doi: 10.1108/14777831111159725.
[94] A. G. Hassan, M. A. Fullen, and D. Oloke, "Problems of drought and its management in Yobe State, Nigeria," *Weather Climate Extremes*, vol. 23, Mar. 2019, Art. no. 100192, doi: 10.1016/j.wace.2019.100192.

Jie Tang received the B.S. degree in geographic information science from Central South University, Changsha, China, in 2021. She is currently working toward the M.S. degree in cartography and geographic information engineering with the Chinese Academy of Surveying and Mapping, Beijing, China.

Her research interests include nighttime light remote sensing and its application in sustainable development.

Xizhi Zhao received the B.S. degree in science of geography and the Ph.D. degree in cartography and geographic information systems from East China Normal University, Shanghai, China, in 2013 and 2019, respectively.

She is currently an Assistant Research Fellow with the Chinese Academy of Surveying and Mapping, Beijing, China. Her research interests include the nighttime light remote sensing and urban remote sensing.

Fuhao Zhang received the B.S. degree in surveying engineering from Tongji University, Shanghai, China, in 1996, and the Ph.D. degree in cartography and geographical information engineering from Liaoning Technical University, Fuxin, China, in 2010.

His research interests include spatial decision science and geospatial big data.

Agen Qiu received the Ph.D. degree in cartography and geographical information engineering from Wuhan University, Wuhan, China, in 2017.

His research interests include spatiotemporal big data analysis and mining, and intelligent modeling of geographic information.

Kunwang Tao received the M.S. degree in cartography and geographical information engineering from the Chinese Academy of Surveying and Mapping, Beijing, China, in 2006.

His research interests include geospatial big data applications and geographic information intelligence services.